

Domain and lattice contributions to dielectric and piezoelectric properties of $\text{Pb}(\text{Zr}_x\text{Ti}_{1-x})\text{O}_3$ thin films as a function of composition

S. Hiboux, P. Muralt, and T. Maeder

Laboratoire de Céramique, Federal Institute of Technology (EPFL), CH-1015 Lausanne, Switzerland

(Received 29 December 1998; accepted 28 July 1999)

In situ reactively sputter deposited, 300-nm-thick $\text{Pb}(\text{Zr}_x\text{Ti}_{1-x})\text{O}_3$ thin films were investigated as a function of composition, texture, and different electrodes (Pt, RuO_2). X-ray diffraction analysis, ferroelectric, dielectric, and piezoelectric measurements were carried out. While for dielectric properties bulklike contributions from lattice as well as from domains are observed, domain wall contributions to piezoelectric properties are very much reduced in the morphotropic phase boundary (MPB) region. Permittivity and d_{33} do not peak at the same composition; the MPB region is broadened up and generally shifted to the tetragonal side.

I. INTRODUCTION

Ferroelectric thin films of the solid solution $\text{Pb}(\text{Zr}_x\text{Ti}_{1-x})\text{O}_3$ (PZT) find a growing interest for applications in nonvolatile memories,^{1,2} microactuators,³ and infrared detectors.^{4,5} As known from bulk ceramics, the properties vary substantially with the compositional parameter x . There is still a lack of knowledge on how properties change as a function of composition in thin films. The most complete work performed to date is the investigation of metalorganic chemical vapor deposition (MOCVD) grown single-crystalline, (100)-oriented PZT films by Foster *et al.*,⁶ covering film morphology, microstructure data, refractive index, dielectric constant, ferroelectric polarization, and coercive field. Piezoelectric properties are not included in this study. In addition, polycrystalline films are more relevant for applications than single-crystal films. They may differ in properties, since domain contributions depend on grain size and microstructure.^{7,8} Apart from application driven interests to find optimal compositions for polycrystalline PZT films,⁹ the variation of concentration may also help to gain a better comprehension of the mechanisms governing PZT thin film properties. The region near the morphotropic phase boundary (MPB), i.e., x near 0.5, is of special interest. This boundary separates the tetragonal symmetry of Ti-rich compositions from the rhombohedral symmetry of Zr-rich compositions. The large number of possible polarization directions at this boundary leads to a peaking of permittivity and piezoelectric coefficients. In bulk PZT this occurs at $x = 0.50$ to 0.52 .¹⁰ Thin films may behave differently in their domain contributions, because of the clamping to the substrate and smaller grains and because of the columnar, often textured microstructure.

It is the scope of the paper to investigate polycrystalline PZT films throughout the compositional range of the solid solution, to characterize also piezoelectric properties, and to address the question of domain contributions. The compositional parameter x (Zr content) was varied between 0.1 and 0.7 in steps of 0.05–0.1. One set of samples consisted of (111)-textured films on platinum electrodes. A second set of samples was grown on RuO_2 electrodes. The PZT thin films of this set exhibit a more or less random orientation.

II. THIN FILM DEPOSITION

PZT thin films were deposited by dynamic *in situ* sputtering from three elemental targets.^{11–13} The Ti and Zr magnetrons were operated with direct-current (dc) power, and the Pb magnetron with radio-frequency (rf) power. The films were grown at 570 °C with a dynamic rate of 3 nm/min, corresponding to about one unit cell per turn of the substrate carrier. The temperature had been previously calibrated with thermocouples. The applied process parameters are given in Table I.

Silicon wafers covered by 1 μm of thermal oxide were utilized as substrates. Two types of bottom electrodes were applied. The (111)-oriented growth was achieved by means of $\text{TiO}_2/\text{Pt}/\text{TiO}_2$ electrodes. The lower 10-nm-thick TiO_2 film served as adhesion layer. It was actually composed of an *in situ* postannealed Ti layer followed by a sputtered TiO_2 layer. The 2-nm-thick top film served as seeding layer for (111)-oriented grains.¹⁴ The 100-nm-thick platinum film was well (111) textured. The second type of electrode consisted of a randomly textured, 300-nm-thick RuO_2 film on a TiO_2 adhesion layer. Samples

TABLE I. Sputter parameters of the PZT deposition process.

Parameters	General conditions
$x = [\text{Zr}]/([\text{Zr}] + [\text{Ti}])$	from 0.1 to 0.7
Lead power supply	rf 150 W
Titanium power supply	dc from 450 to 150 W
Zirconium power supply	dc from 32 to 224 W
Working pressure	16 mtorr pure O ₂ (20 sccm)
Dynamic deposition rate	3 nm/min
Distance targets–substrate	50 mm
Deposition temperature	570 °C
Cooling down	80 mtorr of O ₂ /1 h

of both electrodes were coated in each PZT run. Platinum top electrodes were sputter deposited at room temperature through mechanical masks with round holes of 0.6-mm diameter. Film thickness was controlled by power/time regulation and measured by profilometry (Tencor Alphastep) at chemically etched steps.

The variation of composition was obtained by varying the powers of the Ti and Zr sources. The individual deposition rates for ZrO₂ and TiO₂ films were previously determined at the sputter conditions of the PZT process. The molecular flux ratio of these oxides during the PZT process has been taken as nominal Zr to Ti ratio $[\text{Zr}]/[\text{Ti}]$ of the PZT thin film. The lead stoichiometry was obtained by the self-stabilization of the process. Excess lead was reevaporated.¹¹ For this work, the applied PbO flux was twice as high as the sum of the ZrO₂ and TiO₂ fluxes.

III. CHARACTERIZATION

A. Compositional and structural characterization

A chemical analysis of PZT thin films on RuO₂ (Pt electrodes are less suited as Pb and Pt lines coincide) was carried out by energy dispersive spectroscopy (EDS), together with electron microscopy (Philips XL30), and by x-ray fluorescence (XRF) in a Kevex XRF analyzer. For the compositional range between 10 and 55% Zr content on the B-site (compositional parameter x defined as $x = [\text{Zr}]/([\text{Zr}] + [\text{Ti}])$), both types of measurements (see Fig. 1) yielded a good correspondence between the nominal ratio of Zr to Ti cation concentrations, as defined by the ZrO₂ to TiO₂ flux ratio, and the measured $[\text{Zr}]/[\text{Ti}]$ ratio. At higher concentration, a significant deviation was observed. This indicates either an increased desorption of Zr or a decreased desorption of Ti. A nominal value of 70% Zr content (i.e., $x = [\text{Zr}]/([\text{Zr}] + [\text{Ti}]) = 0.7$) corresponds to a real concentration of rather 60%. In what follows, the nominal value is always indicated as composition.

Film morphology was studied by means of scanning electron microscopy (Philips XL30). The average size of the grains decreased with increasing Zr content from

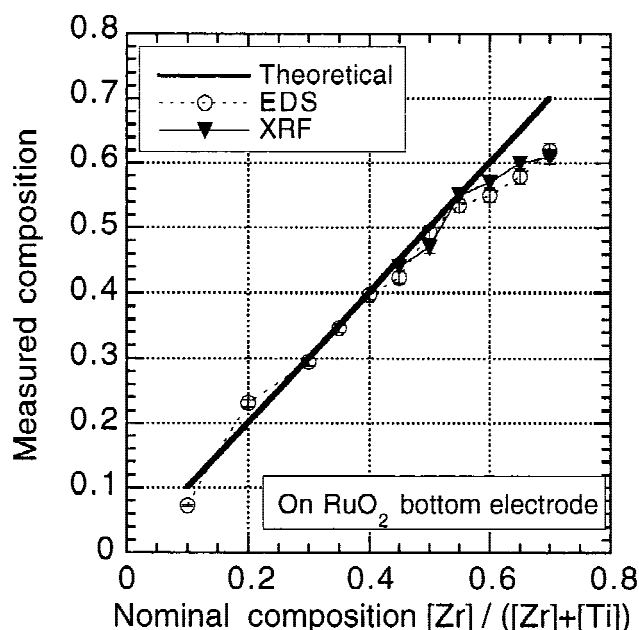


FIG. 1. Chemical analysis of the Zr/Ti ratio in the PZT thin films obtained by XRF and EDS.

200 nm at $x = 0.1$ to 100 nm at $x = 0.7$. The nontextured samples showed a more rough and irregular grain morphology than the (111)-textured layers grown on platinum. The latter exhibited remarkably homogeneous grain sizes at Zr-rich compositions [see Figs. 2(a) and 2(b)].

Film crystallinity and orientation were studied using standard θ – 2θ x-ray diffraction (XRD). Figure 3 shows the x-ray diffraction patterns for PZT on Pt and RuO₂ as a function of the composition (from 10 to 70% of Zr). On Pt(111) the films show a high degree of (111) orientation, whereas on the randomly oriented RuO₂ bottom electrode a random orientation is obtained. No second phases, and especially no pyrochlore, are observed.

The lattice constants a and c of the tetragonal films were extracted from the first-order Bragg peaks (100) and (001), as well as from the second-order Bragg peaks (200) and (002). Whereas the (100) and (200) reflections yield the same a within small limits of ± 0.02 Å, the extraction of c is problematic in the compositional range from 30% to 40% [see Fig. 4(a)]. The $\{00h\}$ peaks are broader and less intense than the $\{h00\}$ peaks. For this reason the (001) and (002) peak positions are probably shifted toward the (100) and (200) peaks. Nevertheless, the tetragonality is lower than in bulk ceramics, especially in the range from $x = 0.3$ to 0.5. At $x = 0.45$ no tetragonal splitting is observed. However, the $\{h00\}$ peaks are still broadened at $x = 0.45$, as compared to the peaks at $x = 0.50$. This allows to conclude that the morphotropic phase boundary is near $x = 0.45$ (nominal composition), instead of $x = 0.52$ as in a bulk ceramic. The concentration measurements suggest that the real Zr concentration at the MPB is even lower, i.e., between

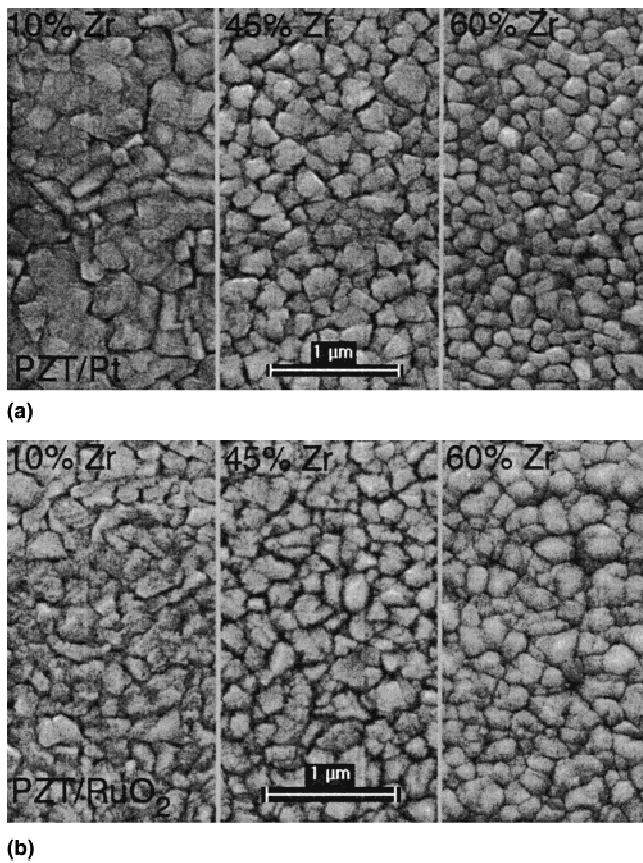


FIG. 2. SEM pictures of PZT thin films with different Zr/Ti ratios: (a) on Pt bottom electrode, (b) on RuO₂ bottom electrode.

$x = 0.42$ and 0.44 . Another difference in bulk ceramics was observed in the spacings of (111) planes ($=d_{111}$). These differ considerably from bulk values in the tetragonal part of compositions [see Fig. 4(b)]. The jump at the morphotropic phase boundary is absent. In contrast, bulk and thin film data are in better agreement at rhombohedral compositions. Thin film data are, however, consistent. The (111) plane spacings from films on Pt(111), from films on RuO₂, and calculated spacings from the a and c parameters of Fig. 4(a) are the same within the experimental errors. The lattice constant a of the rhombohedral compositions is generally found to be higher in thin films than in bulk ceramics.^{6,15} Our data confirm this tendency. Lattice defects⁶ and stresses are thought to cause this shift.¹⁵

The tetragonal distortion is also manifested in the line broadening of higher order x-ray Bragg peaks. Such line broadening of higher order peaks is ascribed to strain variations.¹⁶ With $b_{hkl} = (d_{hkl})^{-1}$ and $\delta b_{hkl} = \cos\theta / \lambda \cdot 2\delta\theta_{hkl}$ where $2\delta\theta_{hkl}$ means the full width at half-maximum (FWHM), a strain variation of $\pm\delta S$ is evaluated according to the following formula:

$$\delta S = \frac{1}{2} \left(\frac{(\delta s_{222})^2 - (\delta s_{111})^2}{s_{222}^2 - s_{111}^2} \right)^{1/2}.$$

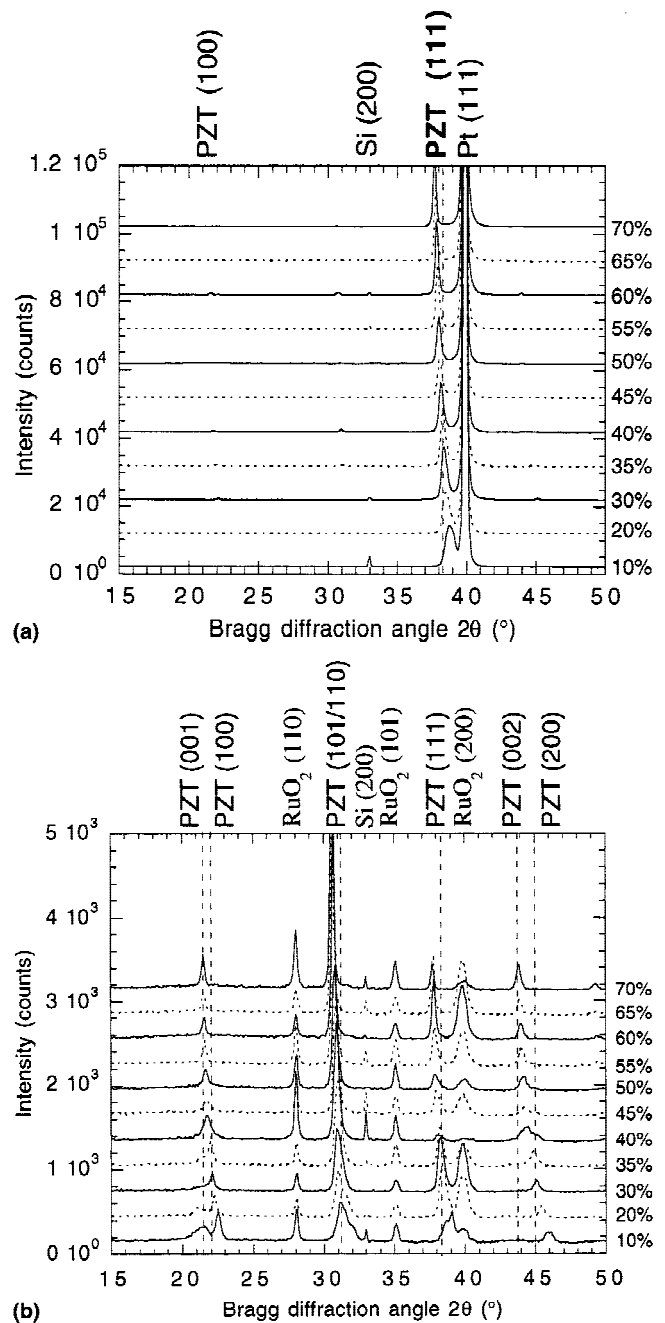


FIG. 3. X-ray θ - 2θ scans for each of the PZT compositions: (a) PZT thin films on platinum electrodes, yielding a dominant (111)-orientation, (b) random PZT thin films on RuO₂ electrodes.

The result of this evaluation is shown in Fig. 5, together with the thin film tetragonality parameter $(a - c)/a$. The strain variation clearly increases with tetragonality and amounts to about 20% of the (theoretical) spontaneous strain. The behavior as a function of composition indicates that the tetragonal phase exists in the range $0 \leq x < 0.4$, since in this range a nearly linear increase of δS with the spontaneous tetragonal strain is observed. Between 0.4 and 0.5 there is a plateau followed by a drop at compositions with rhombohedral symmetry.

B. Ferroelectric and dielectric characterization

Dielectric properties were measured with a HP 4284A impedance analyzer. The polarization was determined with a Sawyer-Tower bridge (RT66A of Radiant Technologies). The piezoelectric coefficient d_{33} was determined with the help of an extremely sensitive double side interferometer described in Refs. 17 and 18.

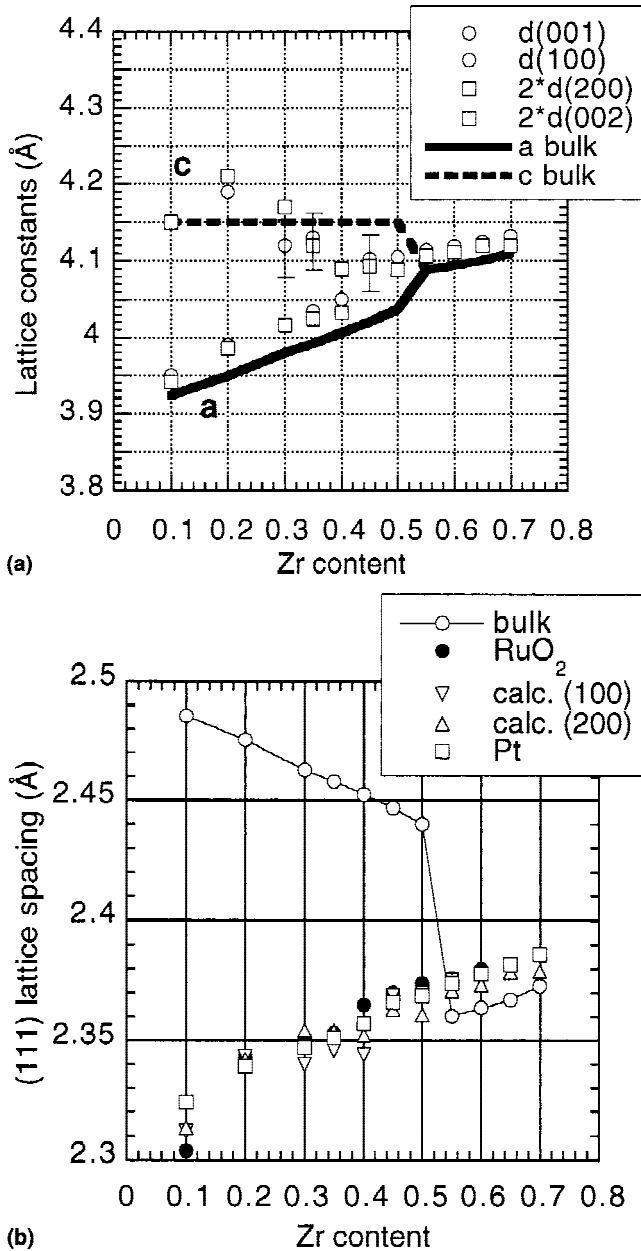


FIG. 4. (a) Lattice constants a and c (tetragonal symmetry) and a (rhombohedral symmetry) derived from $\{n00\}$ reflections of the PZT/ RuO_2 series as a function of composition. The bulk data shown for comparison have been taken from Ref. 31. Lattice spacing between (111) planes, as obtained from (111) Bragg peak positions of x-ray θ - 2θ scans, compared to calculated values derived from the lattice constants [Fig. 4(a)] and bulk data.³¹

The polarization loops were performed with a 100 Hz triangular signal. Figures 6(a) and 6(b) show the polarization hysteresis loops of PZT on Pt as a function of the Zr/Ti ratio. The same measurements have also been made with PZT on RuO_2 bottom electrodes, showing similar behavior. At low Zr concentrations ($x = 0.1$ and $x = 0.2$) only partial switching occurs because the coercive field is too large. This is brought to the fore by the piezoelectric measurements presented later. For $x > 0.2$, the polarization curves show a normal ferroelectric behavior. A negative prepolarization of the films together with a positive voltage shift are observed. Prepolarization and internal bias field will be quantified and discussed later in the context of d_{33} measurement.

Remanent polarizations and coercive fields have been extracted from the polarization curves. They are shown in Figs. 7 and 8 as a function of composition. Note that the values at $x = 0.1$ and $x = 0.2$ do not represent real properties, as no complete switching was achieved.

The remanent polarization increases up to $x = 0.4$, to reach a value close to $30 \mu\text{C}/\text{cm}^2$ on Pt and $25 \mu\text{C}/\text{cm}^2$ on RuO_2 . Negative values are higher than positive ones. For higher Zr concentrations, the values remain constant, except for $x = 0.6$ on Pt, where P_r drops to $20 \mu\text{C}/\text{cm}^2$. The remanent polarization is higher for PZT on Pt bottom electrodes. As for the coercive field, it can be clearly seen that positive values are higher than the negative ones, indicating a negative internal bias field. The minimum coercive field occurs at $x = 0.50$ to 0.55 . Lower E_c values were achieved on Pt bottom electrodes, confirming again superior properties on this electrode.

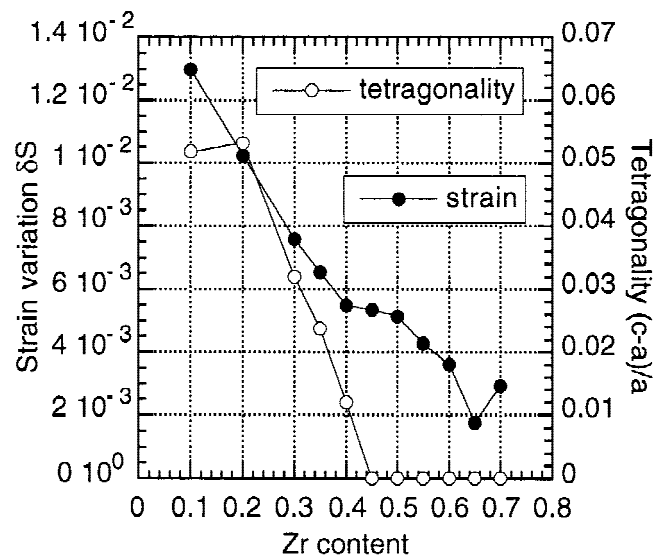


FIG. 5. Strain variation, as derived from the widening of the reciprocal lattice vectors, as a function of composition. The tetragonality parameter $(c - a)/a$ derived from $\{n00\}$ reflections of the PZT/ RuO_2 series [Fig. 4(a)] is shown for reasons of interpretation as well.

The relative permittivity was measured as a function of an applied dc bias field (CV curve). The dc field was varied between ± 300 kV/cm in steps of 1.5 kV/cm at a speed of 1 step/s. The alternating current (ac) field had an amplitude of 5 kV/cm and a frequency of 5 kHz. Figure 9 shows the results as a function of the composition for the case of the PZT/Pt films.

The field dependence of the dielectric constant reflects the contribution of domain walls, which contribute through their oscillation amplitude as well as their density. A peaking occurs near the coercive field due to a

high domain wall density. Upon application of a larger field, domain contributions are reduced as the number of domain walls decreases and as the oscillation amplitudes decrease. In case of low Zr concentrations ($x = 0.1$ and 0.2) there is practically no domain contribution. From $x = 0.3$, the “butterfly” symmetric loops are observed. We can see the increase and then the decrease of the permittivity with the composition, with a maxima for $x = 0.45$. The same tendency is obtained for PZT on RuO_2 but with a maxima for $x = 0.40$. Permittivity measurements thus confirm XRD results and indicate that MPB position at $x = 0.4$ – 0.45 . Figure 10 shows zero-field ($E_{\text{dc}} = 0$) and

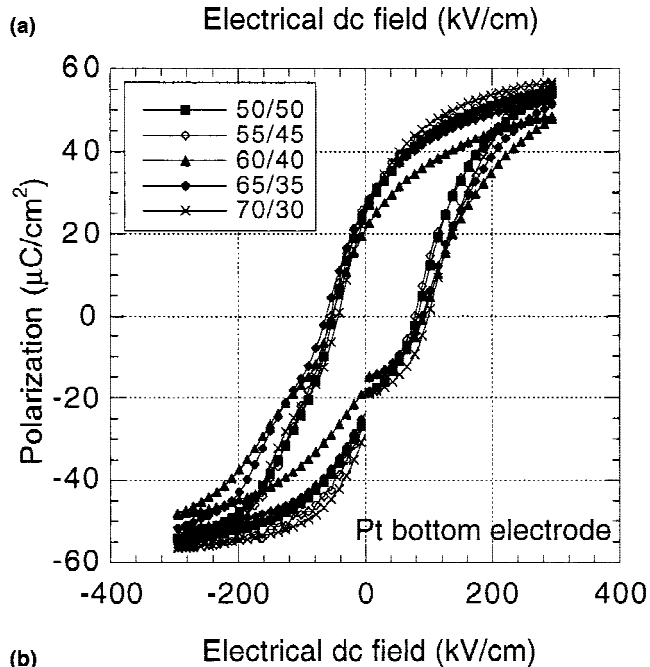
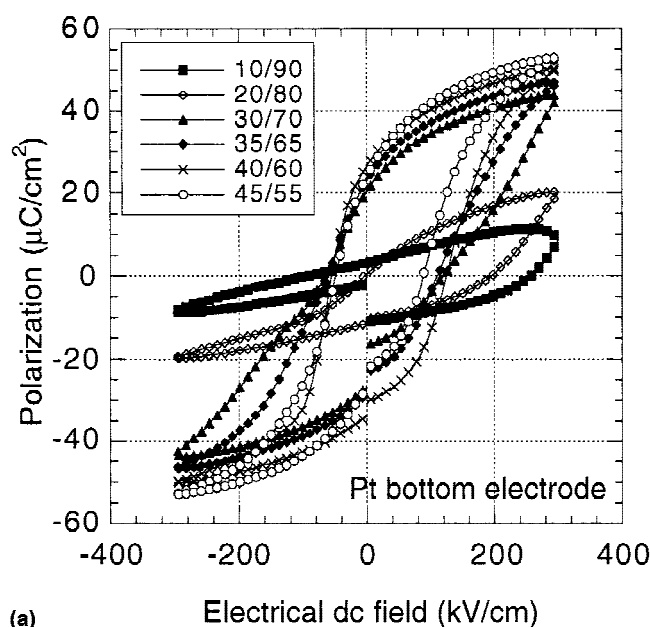


FIG. 6. Polarization hysteresis loops of the PZT films grown on Pt electrodes: (a) the tetragonal side of the composition range, (b) the rhombohedral side of the composition range.

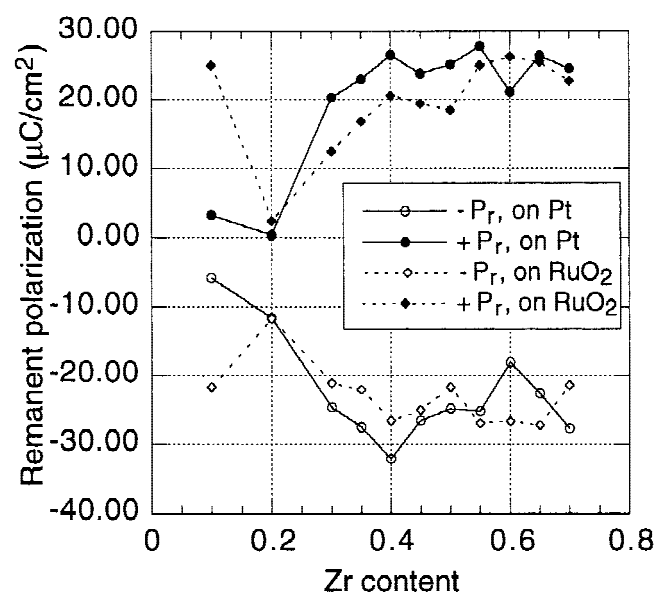


FIG. 7. Remanent polarization as a function of composition.

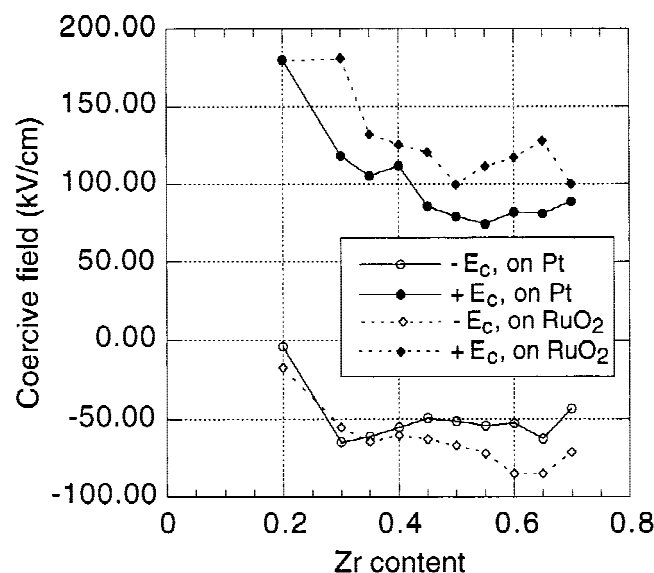


FIG. 8. Coercive field as a function of composition (from polarization measurements).

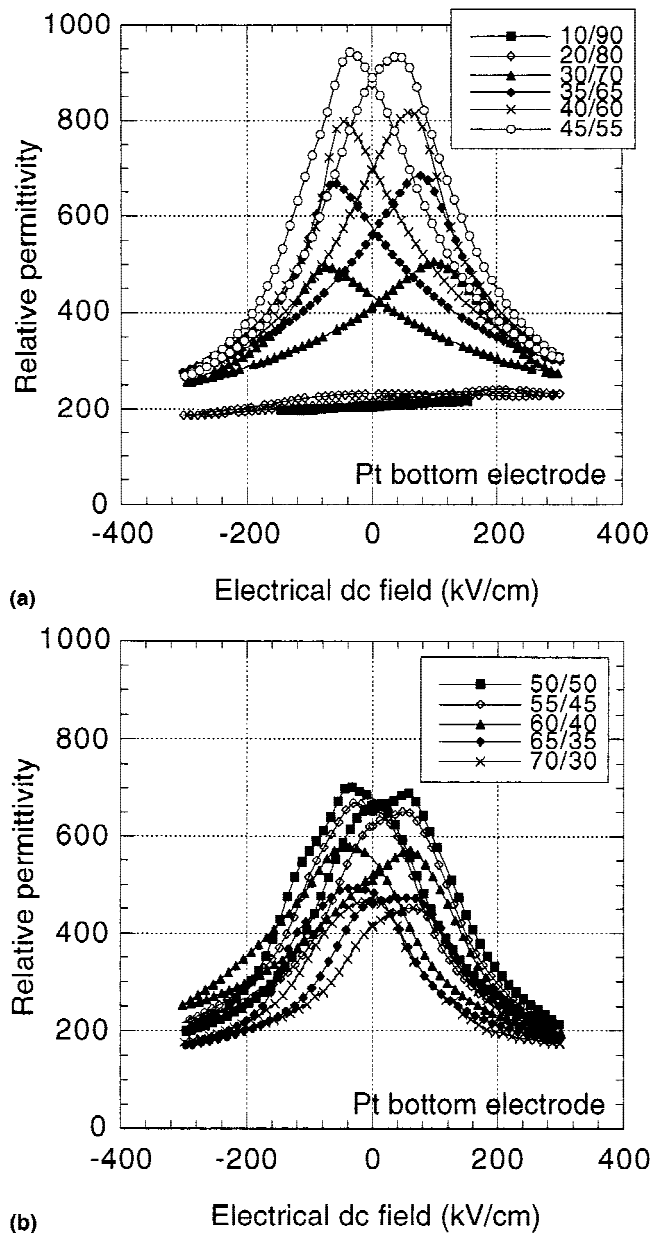


FIG. 9. Relative permittivity for PZT on Pt: (a) the tetragonal side of the composition range, (b) the rhombohedral side of the composition range.

maximum ($E_{dc} = E_c$) values as a function of the composition and the bottom electrode. As in the case of a bulk ceramic,¹⁹ we can observe a peak for the permittivity. The films grown on platinum electrodes exhibit higher values. Zero-field values are of the same order than for an unpoled ceramic ($\epsilon = 800$ for PZT on Pt). The maximum permittivity is obtained when the dc field is close to the coercive one. This increase can reach 20%. The behavior is the same on RuO_2 , except that the maximum value is lower (700 at the unpoled virgin state). For comparison with bulk values, one has to keep in mind that bulk data are measured for constant stress (K_{33}^T) or

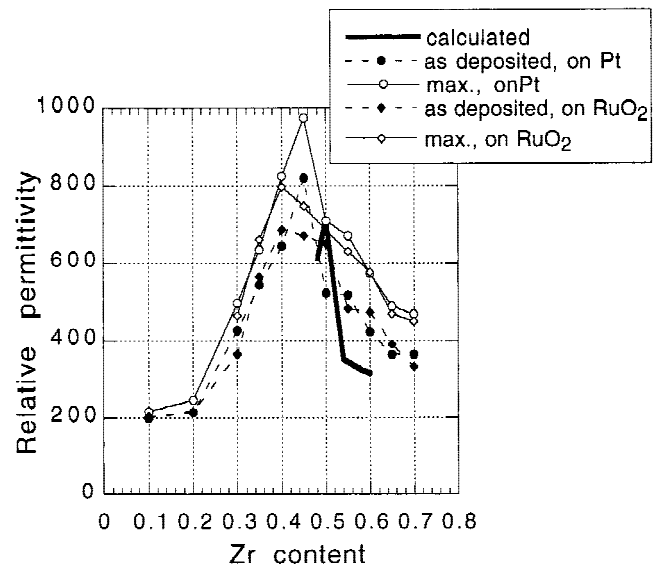


FIG. 10. As-grown (virgin) and maximum relative permittivities as a function of composition. The calculated curve describes the bulk ceramic data,¹⁹ corrected for the clamping effect.

constant strain (K_{33}^S). In case of a thin film on a much thicker substrate, none of these cases applies. The boundary conditions are mixed: constant stress perpendicular to the film plane and constant strain in the film plane. With a complete set of materials coefficients, as published by Berlincourt, Cmolik, and Jaffe,¹⁹ a hypothetical thin film dielectric constant can be calculated as the following:

$$K_{33,f} = K_{33}^T - \frac{2d_{31}^2}{(s_{11}^E + s_{12}^E)\epsilon_0}.$$

The obtained values are depicted in Fig. 10 for comparison. At maximum, the zero-field values are very close or somewhat higher to the so calculated $K_{33,f}$. The peak is, however, much broader and shifted to tetragonal compositions.

C. Piezoelectric coefficient d_{33}

The piezoelectric d_{33} coefficient has been measured as small signal response to a small ac field as a function of a much larger dc field. The same parameters were applied as for the permittivity measurements, i.e., 5 kHz, 5kV/cm, 1.5 kV/cm steps, and 1 step/s. Figures 11(a) and 11(b) show the d_{33} hysteresis loops of PZT on RuO_2 , versus composition. Same measurements have been made on Pt bottom electrode. With such measurements self-poling by the process can be detected, because a nonzero d_{33} means also a nonzero polarization.

For 10% Zr, the switching of domains is incomplete; i.e., the transition through zero polarization is not achieved. The film is strongly negatively polarized. For $x = 0.2$, more but still incomplete switching is observed. This observation is in agreement with the other electrical

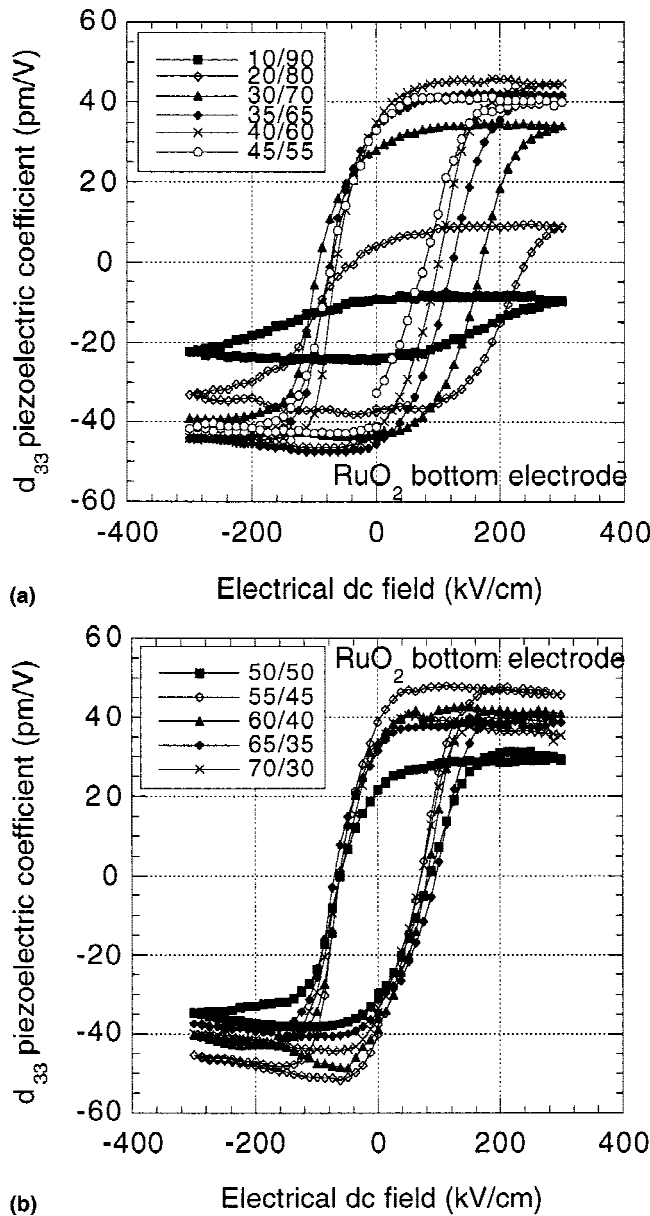


FIG. 11. Effective piezoelectric coefficient $d_{33,f}$ for PZT on RuO_2 : (a) the tetragonal side of the composition range, (b) the rhombohedral side of the composition range.

results seen before. For $x = 0.3$ and higher, the hysteresis loops indicate complete switching, i.e., a normal behavior of a ferroelectric material. However, negative initial values and thus poling by the process are still observed. Figure 12 represents the initial (at the virgin state) and maximum (measured at negative field) d_{33} values, as a function of the composition. It is known that thin film values are reduced with respect to bulk ceramic values because of the clamping to the substrate. The correction can be calculated as follows:²⁰

$$d_{33,f} = d_{33} - \frac{2s_{13}^E}{s_{11}^E + s_{12}^E} d_{31} \quad .$$

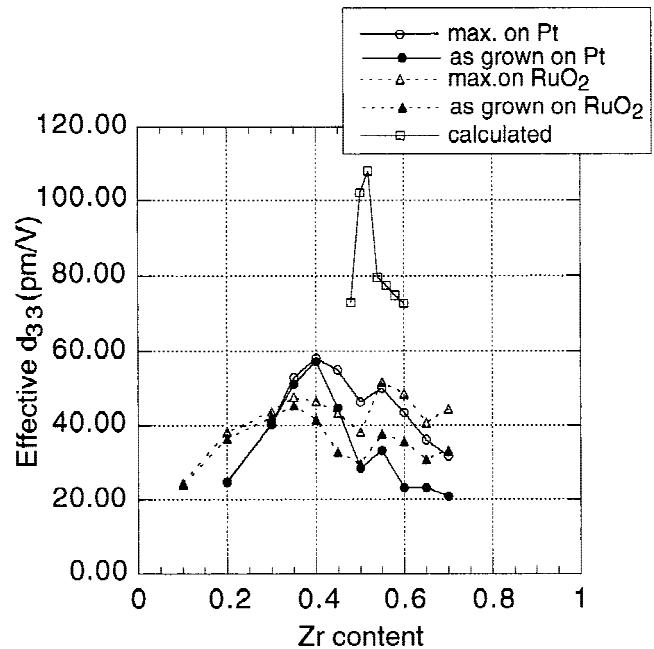


FIG. 12. As-grown (virgin) and maximum of the effective d_{33} piezoelectric coefficient of the PZT films grown on Pt and RuO_2 . The calculated curve describes the available bulk ceramic data,¹⁹ corrected for the clamping effect.

This thin film value $d_{33,f}$, which has been calculated from ceramics data,¹⁰ is also given in Fig. 12.

The measured values are smaller than expected. On Pt electrodes, d_{33} increases with x on the tetragonal side, reaches a maximum for $x = 0.4$ (60 pm/V), and decreases on the rhombohedral side. On RuO_2 , the behavior is quite the same, but the curve is flatter. On this bottom electrode, the values are lower around the maximum area, whereas, for the compositions near PT and PZ, they are higher. A strong similarity can be observed between the initial (virgin) and the maximum values, for each composition. Under $x < 0.4$, maximum values are very close to the initial ones. For $x > 0.4$, initial values are a little bit lower. On Pt electrodes, the maximum is obtained for $x = 0.4$ (in contrast with 0.45 for the permittivity). Once again, the peak in properties is shifted toward Ti richer compositions.

On the basis of these d_{33} measurements, true values for internal and coercive field (slow loop) can be reported [Figs. 13(a) and 13(b)], since—in contrast to hysteresis measurements—the zero polarization state can be located. On both bottom electrodes, high values are observed for tetragonal compositions (for $x = 0.1$ the value is too high to be measurable). The minimum is located between $x = 0.5$ and 0.6 , the values of PZT/Pt being somewhat smaller than the ones of PZT/ RuO_2 .

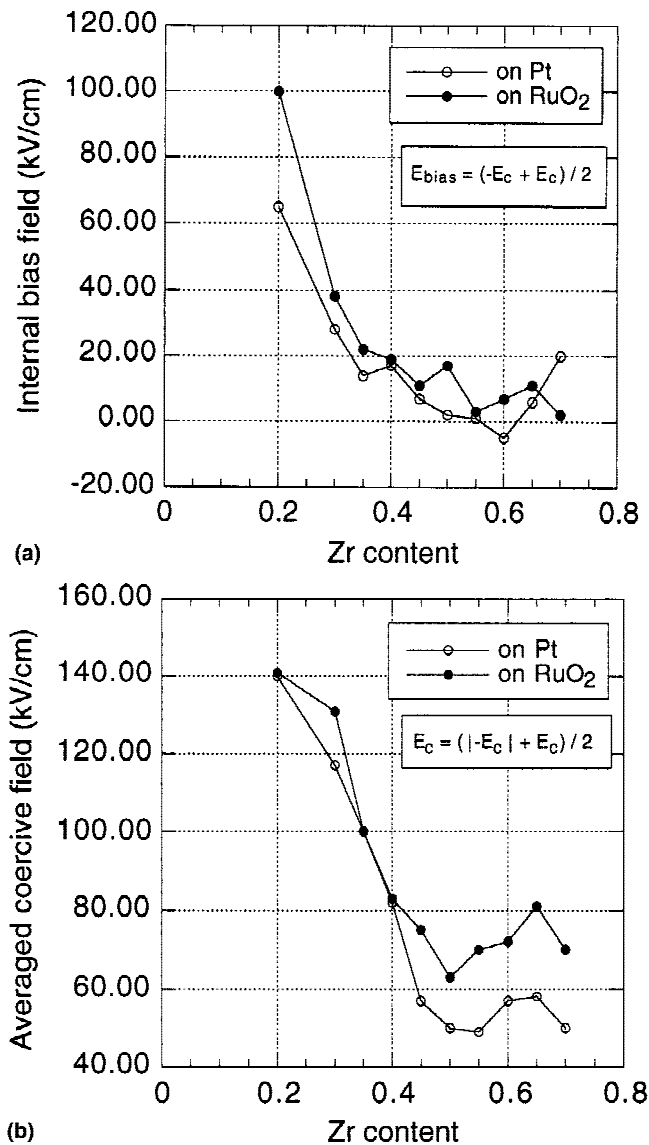


FIG. 13. (a) Internal bias field and (b) averaged coercive field as derived from the d_{33} measurements.

IV. DISCUSSION

A. Lattice and domain contributions

One of the distinct features of ferroelectrics is the fact that dielectric and piezoelectric responses originate from two different mechanisms: first there is a lattice contribution from the displacements of the individual ions (intrinsic contribution) and second there is a contribution from domain wall motions (extrinsic contribution). The latter contribution depends very much on the density and mobility of domain walls. When the small signal response is measured, i.e., the first harmonic to a small alternating electric field, the reversible part of domain wall oscillations is contributing only. The domain wall oscillates so to speak in the bottom of a potential well.

The domain contribution varies with a (much stronger) superimposed dc field. The maximal contribution occurs around the coercive field at the maximal density of domain walls. At high dc fields, the domain wall density is reduced very much and the overall polarization tends toward saturation. The domain contribution is approaching zero, and the lattice contribution is dominating. This is similar to freezing out domain wall oscillations by cooling, as was done for bulk ceramics.²¹

Whereas all domain wall oscillations due to E_{ac} show up in the dielectric response, only the ones that change strains influence the piezoelectric response. A displacement of a 180° domain wall does not modify the strains and thus yields no piezoelectric response. In case of (111)-oriented tetragonal films, even 90° walls should not contribute, as all domains exhibit the same spacing between (111) planes in the stress-free case. We indeed observed that domain wall contributions are very much smaller in the piezoelectric than in the dielectric response. Figure 14 shows a comparison of the two responses for (111)-PZT on platinum as a function of composition. It is evident that the permittivity is very much enhanced by the ferroelectric domain wall motions. The total permittivity achieves values similar to bulk ceramic permittivities. At maximum, the lattice contributes a quarter of the value (250 of 1000). This is in good agreement with low-temperature measurements of bulk ceramics PZT.²² There is, however, less agreement in the case of the d_{33} coefficient. In our (111) thin films the lattice contributes with 66% to the peak value, whereas in bulk ceramics this contribution amounts to 40% only.²² In addition, the intrinsic contribution is reduced near the MPB and enhanced at the other compositions as compared to bulk ceramics (taking into account an approximate reduction for the clamping). No pronounced peaking of the lattice contribution is observed. Since our films are (111)-oriented, one would expect no domain contribution at compositions with tetragonal symmetry. Their peaking at 35–45% indicates that they nevertheless exist. Either the rhombohedral symmetry is still partially present at these compositions or oscillating 90° domain walls between up and down domains somehow couple to strains. This cannot be excluded as there is a tilt angle between the (111)-planes of such neighboring domains. In thin films, such tilting is impossible near the electrode interface. The resulting stresses may yield strains that change the spacing between (111)-planes. Such inhomogeneous strain was shown to exist in the previous section (Fig. 5). Their correlation with tetragonality indicates that the strain inhomogeneity is mostly due to spontaneous strains. Comparison between permittivity and d_{33} leads thus to the conclusion that 180° domain wall oscillations contribute very much to the dielectric constant and show maximum activity at the 45/55 composition. Domain wall oscillations coupling to strains are very

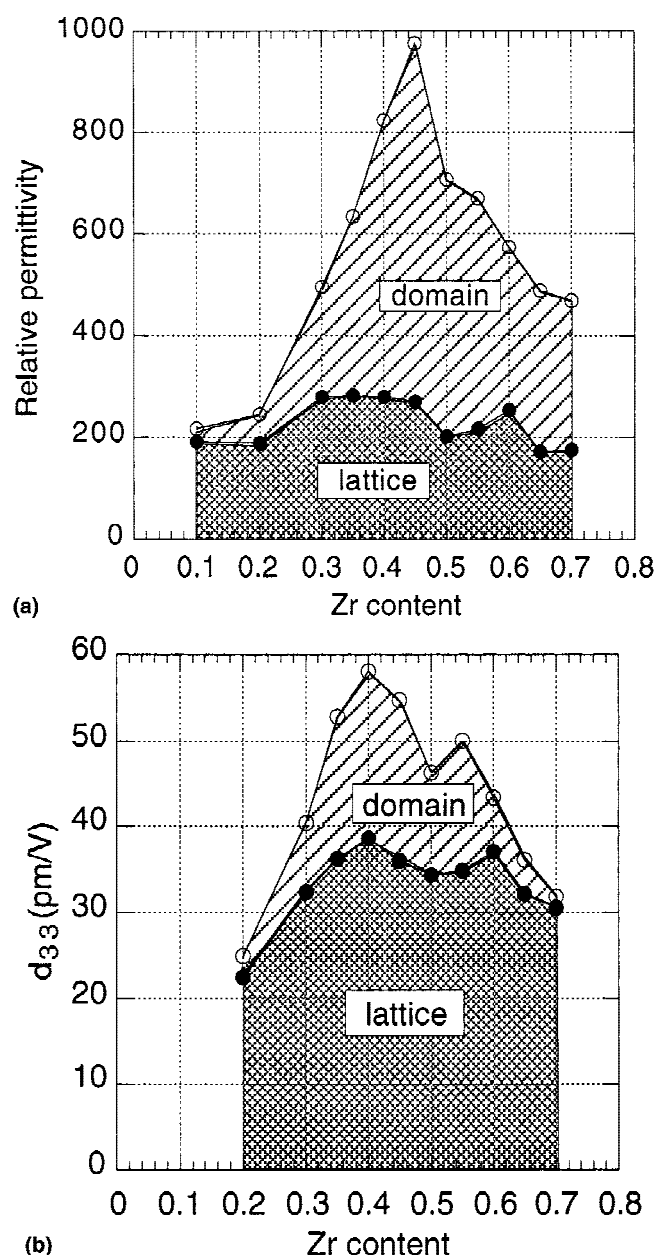


FIG. 14. (a) Permittivity and (b) d_{33} of PZT/Pt films as a function of composition, showing the contributions of lattice and domains effects (the lattice contribution corresponds to the high-field value at 300 kV/cm).

much reduced with respect to bulk ceramics and show a maximum activity at the 40/60 composition. This shift of piezoelectric activity in direction of tetragonal compositions was recently also observed for the e_{31} coefficient.⁹

The random PZT films on RuO₂ electrodes show an even more reduced domain wall contribution. The lattice contribution is about the same. The clamping of domain walls is thus more effective on RuO₂. In intrinsic properties, the two types of PZT thin films do not differ significantly. The effective electrostrictive coefficient

Q_{eff} , as defined by the equation $d_{33} = 2K_{33}\epsilon_0 Q_{\text{eff}} P_3$, has been evaluated for the lattice contributions. For all films, Q_{eff} varies between 0.025 and 0.04 m⁴ C⁻².

The reduction of piezoelectrically active domain wall motions in thin films may have several origins. It was shown for bulk ceramics that domain wall mobility and configuration depend very much on the microstructure of the PZT.⁸ Below a grain size of 1 μm , domains are smaller and charged domain walls are more likely to appear. Furthermore, for small grains, the density of domains increases and so their mobility is reduced. Thin films of PZT predominantly consist of such small grains, at least in less than 1- μm -thick films (the size of the grains in our 300-nm-thick films is less or equal to 300 nm). It has also been shown²³ that 1 μm was the critical thickness below which piezoelectric properties decreased. Further evidence of property reduction is given by the fact that the tetragonality is reduced in the compositional range between 0.3 and 0.5. It is known from BaTiO₃ ceramics⁷ that small grains (<1 μm) have a reduced tetragonality and even show the appearance of an orthorhombic phase. In case of PZT, the critical thickness is rather in the 100-nm size. The clamping to the substrate may inhibit domain wall motions, too. Epitaxial ordering of the PZT lattice on top of the electrode is established in the paraelectric phase. The strong anisotropic stresses imposed by the ferroelectric phase transition might be released partially by dislocations and other defects, which freeze-in the domain pattern at the interface. Alternatively, nano-sized domain patterns might be imposed by the electrode in order to limit strains in the electrode material. Finally, films obtained by physical vapor deposition (PVD) techniques might exhibit a larger amount of oxygen vacancies. These may compensate charges at domain walls, or polarization charges near the interface, during cool down between ferroelectric phase transition and room temperature. The fact that RuO₂ and Pt electrodes lead to different lattice contributions suggests that phenomena at the interface are very crucial.

B. Internal bias field

A pronounced feature of our sputter deposited films is the occurrence of strong internal bias fields, or voltage offsets, which are particularly strong for Ti-rich compositions [see Fig. 13(a)]. This phenomenon has been observed by several groups in case of sputter-deposited films,^{24,25} in plasma-treated films (RIE-etching),²⁶ and in the case of different materials for top and bottom electrodes.²⁷ Except for the latter case, which is explained by differences in the work function of the two metals, such voltage shift is related to nonuniformly distributed oxygen vacancies,²⁷ the formation of dipoles with oxygen vacancies and negatively charged acceptors,²⁸ or also the nonuniform compensation of oxygen vacancies.²⁴ The creation of oxygen vacancies is due to vacuum exposi-

tion at high temperatures, plasma self-bias during etching, and acceptor doping. The finding of Prokopalo²⁹ that the probability of oxygen vacancies increases with the Ti content is in fact compatible with experiments presented in this paper. This effect results in a clamping of the domain walls, which acts against domain motion. In addition to voltage shifts, pinning by space charges at the interfaces leads also to a slanting of the hysteresis loop by screening domains from reorientation.²⁶ The theory of creation of an internal bias field by oxygen vacancies is compatible with our fabrication process, since the sputtered PZT films are grown *in situ* in a low oxygen partial pressure. All these phenomena are indeed in good accordance with the properties we have measured in our films: the coercive field, the voltage offset, and the slanting of the hysteresis loop increase with increasing Ti concentration for concentrations higher than 60%. The role of oxygen vacancies is further supported by the fact that postannealing in oxygen was increasing dielectric and piezoelectric properties, while at the same time the internal bias field and the built-in polarization were reduced (details will be published later).

On the RuO₂ bottom electrode, the tendency is the same as that on Pt, but the internal bias field is higher on this electrode. This effect can be explained by the asymmetry of the electrical contacts (the top electrode is always Pt), which yields a difference in the built-in voltages at the two different interfaces.

C. Coercive field

Figure 15 shows the positive, negative, and averaged coercive fields, taken from polarization, dielectric, and piezoelectric measurements. Similar to the internal bias field, the coercive fields decrease with increasing Zr. This tendency is also observed in PZT thin films by Foster,⁶ Takayama,²⁵ and Hector.¹⁵ Compared to bulk ceramics, coercive fields are much higher in thin films. This effect may be due to the same reasons as described above for the internal bias field, i.e., clamping of domains by dipolar or charged defects, large stresses in the film, and small grain sizes. One can see that the different methods for measuring E_c yield different results. When E_c is derived from the polarization loop, which is captured within 10 ms, transient phenomena influence the experiment. In contrast, coercive fields derived from C-V curvelike measurements (thus permittivity and d_{33}) reflect a quasi-static situation. There is nevertheless a difference between $E_c(\epsilon_{33})$ and $E_c(d_{33})$: at the first field the domain density is maximal; at the second field the average polarization is zero. Our measurement shows that the maximal domain wall density is achieved before the average polarization has reached zero. The dynamic E_c from polarization loops is generally larger than the two

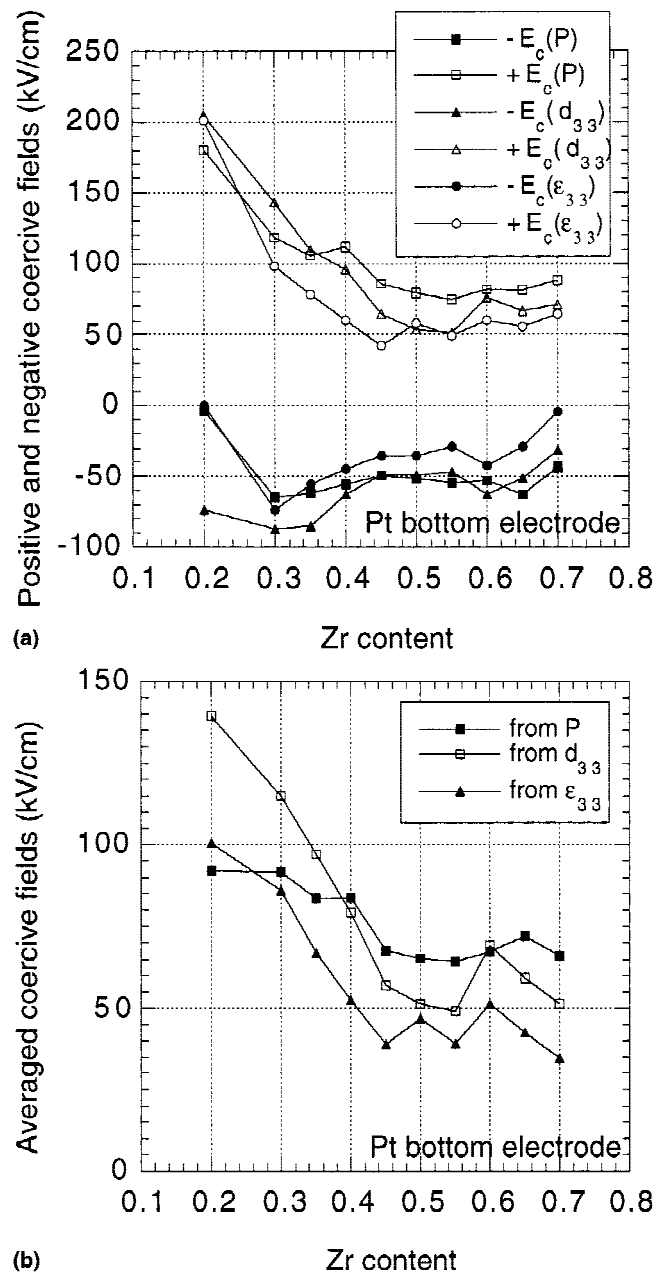


FIG. 15. Coercive fields from small signal response measurements (d_{33} permittivity) and from the polarization hysteresis loops. In (a) the positive and negative values are shown; in (b) the averaged values are shown.

other ones. However, for Ti-rich compositions a too low value is obtained due to strong backswitching of domains.

D. Phase transitions

There is evidence from dielectric and piezoelectric properties as well as from XRD data that the MPB is shifted toward the tetragonal side by 5–10%. Previous studies performed so far with epitaxial films^{6,25} and by polycrystalline sol-gel films¹⁵ confirmed the usual MPB

composition within a precision of 5%. These studies, however, did not include piezoelectric properties, which apparently are more sensitive to microstructural features than dielectric properties. A recent study on sol-gel-processed PZT thin films revealed that the effective piezoelectric coefficient $e_{31,f}$ was peaking at lower Zr concentrations (i.e., at $x = 0.45$) than the permittivity or $d_{33,f}$ (i.e., at 53/47).⁹ The evaluation of intrinsic and extrinsic contributions (see Fig. 14) shows that intrinsic contributions peak at $x = 0.40$, whereas the strongest extrinsic contributions are seen in the dielectric response at $x = 0.45$. This contribution is most likely due to 180° domain wall motions, because otherwise it should also be seen in the piezoelectric response. In the latter, the extrinsic contribution is equal for $x = 0.4$ and $x = 0.45$. The origin of the different positions of the peaks lies thus in different composition dependencies of intrinsic and the various extrinsic contributions.

One particular behavior we have also observed in our thin films is the presence of a second peak in d_{33} and K_{33} appearing at $x = 0.55$ for extrinsic and $x = 0.60$ for intrinsic contributions (see Fig. 14), which, to our knowledge was never observed before. These compositions come quite close to the normal MPB compositions when taking into account the compositional correction. It could be that our films exhibit a morphotropic phase boundary region which is very much extended as compared to large grain materials. Instead of one peak, two peaks would appear. Alternatively, the second peak could be due to the transition between the high-temperature and low-temperature rhombohedral phase, which would lead to improved properties because of multiple cell contributions in this phase.¹⁰ More investigations are needed to clarify the origin of this second peak.

Independently of the open origin of the second peak it is clear that the phase transition at the morphotropic phase boundary (RH-T) is broadened. The peak of the dielectric constant is much wider than in bulk ceramics, a reduction of tetragonality occurs, and piezoelectric properties are reduced inside the MPB region. The intrinsic properties, such as the electrostrictive coefficient, are, however, relatively uniform as a function of composition. There is thus a large reduction of piezoelectrically active domain wall motions in the MPB zone. This is understandable for (111)-oriented films in the tetragonal phase. However, the random oriented films on RuO₂ show that this explanation does not hold, as these films show even less domain activity than the (111) films on platinum. One is thus left with the possibility that the interface to the bottom electrode plays the major role. During nucleation of the film, this interface has a major influence on the final grains size. The elastic and plastic properties and the thermal expansion coefficients of the electrode materials should have a major influence on how 90° domain patterns accommodate the electrode. In

addition, the ability to neutralize charged domain walls may play a role too. The broadening of the MPB transition and the reduction of 90° domain wall motions can thus be understood as a combination of the effects of small grains, large stresses (mostly inhomogeneous) due to impossible stress relaxation at the interface, and pinning of domain walls by defect.

The role of the average stress is not as important (measured about 100 MPa tensile at 45/55 composition). However, the strain variation yields much more local stresses of several 100 MPa up to a few GPa, taking into account a biaxial of modulus of about 100 GPa. Piezoelectric couplings between order parameter (i.e., the polarization components P_1 , P_2 , and P_3) and shear stress components X_4 , X_5 , and X_6 (crystal frame) may yield a broadening of the transition. This coupling is written in the crystal frame as follows (see e.g., Ref. 30):

$$-Q_{44}[X_4P_2P_3 + X_5P_1P_3 + X_6P_1P_2] \quad .$$

For the (111) textured films, this coupling term leads also to couplings with nonshear stress components defined in the film frame. A uniform film stress σ_f in the plane of the film leads to the following piezoelectric coupling term:

$$\frac{1}{3}Q_{44}[P_2P_3 + P_1P_3 + P_1P_2]\sigma_f \quad .$$

Q_{44} is positive and quite large. A compressive stress thus would stabilize the solution $P_1 = P_2 = P_3$, thus the rhombohedral case. Tensile stress stabilizes other rhombohedral solutions ($P_1 = P_2 = -P_3$) or new solutions with two P -components different from zero and one zero (orthorhombic). The coupling to stress may also account for the shift of the phase transition. One may argue that the local stress that develops due to clamping and the ferroelectric phase transition always opposes the increase of the tetragonal c axis along the in-plane directions, thus increasing the free energy of the tetragonal solution for all orientations. The difference from thicker films prepared by sol-gel techniques, where no shift of MPB is observed (more precisely, d_{33} and K_{33} do not show a shift, but the e_{31} peak is shifted to the tetragonal side⁹), is possibly a more relaxed film/Pt interface and a larger grains size.

V. CONCLUSION

Pb(Zr_{*x*}Ti_{*1-x*})O₃ thin films have been deposited by *in situ* reactive sputtering. The obtained films do not contain second phases. The compositional parameter was varied between 0.1 and 0.7. Two series of 300-nm-thick films have been fabricated. One consisted of (111)-textured films on platinum electrodes, the other of randomly oriented films on RuO₂ electrodes. The permittivity is measured to be as high as in bulk ceramics, while a strong reduction in d_{33} is observed, even

when taking into account the clamping by the substrate. Small signal response measurements as a function of the dc electrical field allowed one to separate lattice and domain wall contributions. It is the domain wall contribution which is very much reduced in the case of piezoelectric properties, while for dielectric properties bulklike contributions are observed. This allows one to conclude that the piezoelectrically active 90° domains are hindered in their motion or do not exist as abundantly as in large-grained bulk ceramics. As a further consequence, the maximum dielectric and piezoelectric responses are not found at the same Zr contents. The latter is shifted by $\Delta x = -0.05$ toward tetragonal compositions. The morphotropic phase boundary is found to be shifted toward tetragonal compositions. X-ray line width measurements indicate a broadened transition zone between $x = 0.40$ and 0.50 . They also reveal large inhomogeneous strains, which increase with increasing tetragonality. These strains result mainly from the clamping to the electrode.

Coercive field and voltage shift increase strongly with increasing Ti content or tetragonality. The growing inhomogeneous strains might be one reason for that. On the other hand, the ability to form oxygen vacancies increases also with a higher Ti content. The lowering of coercive field and voltage shift by annealing in oxygen suggests indeed that domain pinning by oxygen defects play an important role. A third important parameter is the grain size, as known from literature on bulk ceramics. With an average diameter of 150 nm at MPB compositions, the grain size is critical; i.e., domain configurations are limited to laminar structures with limited possibility to relax stresses.

The main difference between the two series is the smaller domain wall contributions in films grown on RuO_2 . The lattice contribution to piezoelectricity are about equal. A puzzling point was discovered in (111)-oriented PZT thin films on platinum. For tetragonal symmetry, 90° domains should be equivalent with respect to strains in the [111] direction. However, they show a larger domain wall contribution than the random films on RuO_2 . The influence of the electrodes and the symmetries present in the widened MPB region need to be clarified in future work.

ACKNOWLEDGMENT

This work was supported by the Swiss Priority Program on Materials Research (PPM).

REFERENCES

1. C.A. Araujo, L.D. MacMillan, B.M. Melnick, J.D. Cuchiaro, and J.F. Scott, *Ferroelectrics* **104**, 241 (1990).
2. R.E. Jones, P. Zürcher, P. Chou, D.J. Taylor, Y.T. Lii, B. Jiang, P.D. Maniar, and S.J. Gillespie, *Microelectron. Eng.* **29**, 3 (1995).
3. P. Muralt, M. Kohli, T. Maeder, A. Kholkin, K.G. Brooks, N. Setter, and R. Luthier, *Sens. Actuators A* **48**, 157 (1995).
4. R. Bruchhaus, *Ferroelectrics* **133**, 73 (1992).
5. M. Kohli, C. Wüthrich, K.G. Brooks, B. Willing, M. Forster, P. Muralt, N. Setter, and P. Ryser, *Sens. Actuators A* **60**, 147 (1997).
6. C.M. Foster, G-R. Bai, R. Csencsits, J. Vetrone, R. Jammy, L.A. Wills, E. Carr, and J. Amano, *J. Appl. Phys.* **81**, 2349 (1997).
7. G. Arlt, D. Hennings, and G. de Witt, *J. Appl. Phys.* **58**, 1619 (1985).
8. G. Arlt, *Ferroelectrics* **91**, 3 (1989).
9. M-A. Dubois, P. Muralt, D.V. Taylor, and S. Hiboux, *Integr. Ferroelectr.* **22**, 535 (1998).
10. B. Jaffe, W.R. Cook, and H. Jaffe, *Piezoelectric Ceramics* (Academic Press, London, 1971).
11. T. Maeder, P. Muralt, M. Kohli, A. Kholkin, and N. Setter, *Br. Ceram. Proc.* **54**, 206 (1995).
12. T. Maeder and P. Muralt, in *Epitaxial Oxide Thin Films and Heterostructures*, edited by D.K. Fork, J.M. Phillips, R. Ramesh, and R.M. Wolf (Mater. Res. Soc. Symp. Proc. **341**, Pittsburgh, PA, 1994), pp. 361–366.
13. R. Bruchhaus, H. Huber, D. Peitzer, and W. Wersing, *Integr. Ferroelectr.* **2**, 157 (1992).
14. P. Muralt, T. Maeder, L. Sagalowicz, S. Hiboux, S. Scalese, D. Naumovic, R.G. Agostino, N. Xanthopoulos, H.J. Mathieu, L. Patthey, and E.L. Bullock, *J. Appl. Phys.* **83**, 3835 (1998).
15. H. Hector, N. Floquet, J.C. Niepce, P. Gaucher, and J.P. Ganne, *Microelectron. Eng.* **29**, 285 (1995).
16. B.E. Warren and B.I. Auerbach, *J. Appl. Phys.* **21**, 595 (1950).
17. A. Kholkin, E. Colla, K. Brooks, P. Muralt, M. Kohli, T. Maeder, D. Taylor, and N. Setter, *Microelectron. Eng.* **29**, 261 (1995).
18. A.L. Kholkin, Ch. Wüthrich, D.V. Taylor, and N. Setter, *Rev. Sci. Instrum.* **67**, 1935 (1996).
19. D.A. Berlincourt, C. Cmolik, and H. Jaffe, *Proceedings of the IRE* (Institute of Radio Engineers, New York, 1960), Vol. 48, pp. 220–229.
20. K. Lefki and G.J.M. Dormans, *J. Appl. Phys.* **76**, 1764 (1994).
21. X.L. Zhang, Z.X. Chen, L.E. Cross, and W.A. Schulze, *J. Mater. Sci.* **18**, 968 (1983).
22. Z.Q. Zhuang, M.J. Haun, S-J. Jang, and L.E. Cross, *IEEE Trans. UFFC* **36**, 413 (1989).
23. S. Trolier-McKinstry, P. Aungkavattana, F. Chu, J. Lacey, J-P. Maria, J.F. Shepard, Jr., T. Su, and F. Xu, in *Ferroelectric Thin Films VI*, edited by R.E. Treece, R.E. Jones, C.M. Forster, S.B. Desu, and I.K. Yoo (Mater. Res. Soc. Symp. Proc. **493**, Pittsburgh, PA, 1998), pp. 59–68.
24. G.E. Pike, W.L. Warren, D. Dimos, B.A. Tuttle, R. Ramesh, J. Lee, V.G. Keramidas, and J.T. Evans, *Appl. Phys. Lett.* **66**, 484 (1995).
25. R. Takayama and Y. Tomita, *J. Appl. Phys.* **65**, 1666 (1989).
26. E.G. Lee, D.J. Wouters, G. Willems, and H.E. Maes, *Appl. Phys. Lett.* **70**, 2404 (1997).
27. J. Lee, C.H. Choi, B.H. Park, T.W. Noh, and J.K. Lee, *Appl. Phys. Lett.* **72**, 3380 (1998).
28. K. Carl and K.H. Härdtl, *Ferroelectrics* **17**, 473 (1978).
29. O.I. Prokopalov, *Sov. Phys. Solid State* **21**, 1768 (1980).
30. M.J. Haun, E. Furmann, S.J. Jang, and L.E. Cross, *Ferroelectrics* **99**, 13 (1989).
31. V.V. Eremkin, V.G. Smotrakov, and E.G. Fesenko, *Ferroelectrics* **110**, 137 (1990).